PCCP

PAPER

Cite this: *Phys. Chem. Chem. Phys.*, 2016, **18**, 12323

Interaction between copper and carbon nanotubes triggers their mutual role in the enhanced photodegradation of *p*-chloroaniline†

N. F. Khusnun,[a] A. A. Jalil,*[ab] S. Triwahyono,[c] N. W. C. Jusoh,[d] A. Johari[ab] and K. Kidam[ab]

Received 31st December 2015,
Accepted 28th March 2016

DOI: 10.1039/c5cp08068a

www.rsc.org/pccp

Copper (Cu, 1–5 wt%) was loaded onto carbon nanotubes (CNTs) by a simple electrochemical method. The physicochemical properties of catalysts (Cu/CNTs) were characterized by using X-ray diffraction (XRD), transmission electron microscopy (TEM), nitrogen (N_2) adsorption–desorption, Fourier transform infra-red spectroscopy (FTIR), X-ray photoelectron spectroscopy (XPS), and electron spinning resonance (ESR). The results showed that the Cu was distributed well on the CNT surface by the interaction of Cu^{2+} ions with –OH and –COOH groups on the CNT surface, which preferentially occurred at the defect sites along the CNT backbone. The Cu–O–C bonds formed were found to play an important role in enhancing the photoactivity of the catalysts. The highest number of Cu–O–C bonds possessed by 3 wt% Cu/CNTs demonstrated the best performance in the degradation of *p*-chloroaniline (96%) under UV light irradiation within 5 h of reaction at 27 °C and under neutral pH conditions. Kinetic studies showed that the degradation followed the pseudo-first order model and the surface reaction was the controlling step. It is believed that these results could contribute to the synthesis of various supported catalysts for various applications.

Introduction

Chlorinated *p*-chloroaniline (PCA) is widely used as an intermediate during the manufacture of a variety of chemicals, including agricultural chemicals, plastics, azo dyes and pigments, and in the production of synthetic organic chemicals and polymers, rubber additives, pharmaceuticals, cosmetic products, pesticides and herbicides, and drugs.[1,2] The widespread use of these compounds has resulted in its presence in the industrial effluent, sludge and agricultural soil. As one of the most persistent organic pollutants widely distributed in the environment, PCA is a priority toxic pollutant that has imposed a serious risk to public health and the environment.[3,4] Thus, several technologies such as biodegradation, radiochemical methods, and adsorption have been developed to degrade this compound.[5–7] However, their application has been limited due to high cost and time-consuming use, as well as production of secondary wastes of some persistent organic pollutants.

Photocatalytic degradation has also become one of the promising techniques for the removal of organic pollutants due to the complete conversion of the pollutants to water and carbon dioxide.[8] Among the catalysts used, TiO_2 is the most popular one but fast electron–hole recombination always suppresses its efficiency. Hybridization of TiO_2 with other nanometal oxides such as ZnO, Fe_2O_3, CuO, ZrO_2, CdS, and SnO_2 as well as supporting TiO_2 on several mesoporous materials such as silica, zeolite and alumina have been among the efforts to overcome the above problem.[9–12] Recently, carbon materials, particularly carbon nanotubes (CNTs), have also been used as supports for various semiconductor photocatalysts due to their interesting features such as high surface area, good anion and cation adsorption, good mechanical properties, and high chemical and thermal stability.[3,13] However, information on the most important aspects addressing the behavior of individual metal ions in or on CNTs, particularly in possible chemical interactions between both, is still lacking and is of interest. Understanding this behavior would lead to the design and synthesis of superior and efficient catalysts for various applications.

Previously, we reported a simple *in situ* electrochemical method for preparing various metal nanoparticles such as α-Fe_2O_3, CuO,

[a] *Department of Chemical Engineering, Faculty of Chemical and Energy Engineering, Universiti Teknologi Malaysia, 81310 UTM Johor Bahru, Johor, Malaysia. E-mail: aishahaj@utm.my*
[b] *Centre of Hydrogen Energy, Institute of Future Energy, Universiti Teknologi Malaysia, 81310 UTM Johor Bahru, Johor, Malaysia*
[c] *Department of Chemistry, Faculty of Science, Universiti Teknologi Malaysia, 81310 UTM Johor Bahru, Johor, Malaysia*
[d] *Department of Environmental Engineering & Green Technology, Malaysia-Japan International Institute of Technology, Universiti Teknologi Malaysia Kuala Lumpur, 54100 Kuala Lumpur, Malaysia*

† Electronic supplementary information (ESI) available. See DOI: 10.1039/c5cp08068a

and ZnO supported on zeolites and silica.[14–16] Besides the formation of metallic nanoparticles, metal ions incorporated in the supports were also discovered during electrolysis, resulting in photocatalysts with high potential for efficient decolorization of various dyes. Hypothesizing that a similar interaction would also occur between metal ions and CNTs when using the same preparation method, herein we report for the first time electrochemically prepared Cu ions supported on multi-walled carbon nanotubes (MWCNTs) and their photoactivity in the degradation of PCA. Cu was chosen as a model metal system due to its completely filled d-orbitals which show low affinity for carbon.[17] The properties of the catalysts were characterized in detail by XRD, TEM, N_2 adsorption–desorption, FTIR, XPS, and ESR. The photocatalytic performance, kinetic studies, proposed structures and mechanisms of the catalysts and photocatalytic reaction are also discussed.

Experimental

Material

Multiwalled carbon nanotubes (MWCNTs) with a diameter of 10–20 nm and a length of 10–50 nm were purchased from Chengdu Organic Chemicals Co., Ltd (China). *N*,*N*-Dimethylformamide (DMF) was obtained from J. T. Baker and naphthalene was obtained from Fluka. Copper (Cu) and platinum (Pt) plates were purchased from Nilaco, Japan. Sodium hydroxide (NaOH) and hydrochloric acid (HCl) were obtained from Merck. *p*-Chloroaniline (PCA) was obtained from Acros. Deionized water was used for the preparation of the pH solution. All chemicals were used as received without treatment.

Synthesis of catalysts

The Cu/CNT composite samples were prepared using an *in situ* preparation technique.[18–20] 15 mL of DMF solution was added to a normal one-compartment cell fitted with a Pt plate (2 cm × 2 cm) cathode and a Cu plate (2 cm × 2 cm) anode which contains 0.1 M TEAP, a naphthalene mediator (1.66 mmol) and CNTs (1 g). Then, electrolysis was conducted at a constant current density of 120 mA cm^{-2} and by continuously stirring under an argon atmosphere. After electrolysis, the sample was impregnated, oven dried overnight at 105 °C, and calcined at 300 °C for 3 h. The required weight of copper loading on the CNT support was calculated based on Faraday's law of electrolysis, as shown in eqn (1),

$$n = \left(\frac{It}{F}\right)\left(\frac{1}{z}\right) \quad (1)$$

where n is the number of moles of Cu, I is the constant current of electrolysis (A), t is the total time the constant current was applied (s), F is the Faraday constant (96 486 C mol^{-1}), and z is the valence number of ions of the substance (electrons transferred per ion). The as-prepared catalysts were obtained and ready to be characterized and subjected to reaction testing.

Characterization

The crystalline structure of the catalyst was studied by X-ray diffraction (XRD) performed on a Bruker Advance D8 X-ray powder diffractometer using Cu Kα radiation at a 2 theta angle ranging from 20° to 80°. The phases were identified with the aid of the Joint Committee on Powder Diffraction Standards (JCPDS) files.

The morphology of the catalyst was characterized by transmission electron Microscopy (TEM) using a JEOL JEM-2100F microscope. The samples were ultrasonically dispersed in acetone and deposited on an amorphous and porous carbon grid. The textural properties (*i.e.*, specific surface area, pore volume, and pore diameter) were determined by nitrogen physisorption at 77 K using a Quantachome Autosorb-1 analyzer. Specific surface area (S_{BET}) values were calculated from the BET isotherm plots, while the total pore volume was calculated using the Barrett, Joyner, and Halenda (BJH) method and pore size distributions were calculated using the Non-Local Density Functional Theory (NLDFT) from the adsorption isotherm.

The chemical functional groups present in the catalyst were identified by FT-IR (Perkin Elmer Spectrum GX FTIR Spectrometer) using the KBr method with a scan range of 400–4000 cm^{-1}. The element composition of the catalyst was investigated using X-ray photoelectron spectroscopy (XPS) conducted on a Kratos Ultra spectrometer equipped with a Mg Kα radiation source (10 mA, 15 kV) in the range of 0–800 eV. The powdered sample was pressed into a small Inox cylinder and analyzed inside an analysis chamber at 1×10^{-10} Pa during data acquisition. To correct the energy shift due to surface charging of the samples, the binding energy of the C1s peak at 284.5 ± 0.1 eV was taken as the internal standard. The electron spinning resonance (ESR) spectra were recorded at room temperature using a JEOL JES-FA100 ESR spectrometer to identify the electronic structure of the catalyst.

Photodegradation of PCA

The photoactivities of the CuO and Cu/CNT catalyst were tested in the photodegradation of PCA. The photocatalytic reaction was experimented in a batch reactor fixed with a UV lamp (4 × 9 W; 365 nm emission). 0.375 g L^{-1} of the catalyst was added to PCA solution with desired concentration (10 mg L^{-1}) and stirred for 1 h in the dark to achieve adsorption–desorption equilibrium. The initial pH of PCA solution was 7 and it was carried out at 27 °C. Then, the reaction was carried out for another 5 h under ultraviolet (UV) light irradiation. The concentration of PCA prior to irradiation was used as the initial value for the PCA degradation measurements. The samples were then collected at a regular interval of 1 h and centrifuged in a Beckman Coulter Microfuge 16 centrifuge at 14 000 rpm for 10 minutes before being analyzed using a UV-Vis Spectrophotometer (Agilent Technology Carry 60 UV-Vis) for the residual concentration of PCA. PCA degradation was measured at the maximum adsorption peak at 239 nm.[21] The degradation percentage was calculated using eqn (2).

$$\text{Degradation (\%)} = \frac{(C_0 - C_t)}{C_0} \times 100 \quad (2)$$

where C_0 and C_t are the initial concentration of PCA and the concentration at time t, respectively. An Agilent Technologies

7820A gas chromatograph coupled with an Agilent Technologies 5977E mass spectrometer detector was used for detection of intermediates formed during photodegradation of PCA for the proposed mechanism.

Results and discussion

Crystallinity, phase and structural properties of the catalysts

The crystallinity of the catalysts was characterized by XRD and their diffractograms in the range of 2θ = 20–80° are shown in Fig. 1. The electrosynthesized CuO nanoparticles showed characteristic peaks for the pure monoclinic structure of CuO (JCPDS 48-1548) at 32.5°, 35.5°, 38.7°, 48.8°, 53.4°, 58.2°, 61.5°, 65.8°, 67.9°, 72.4°, and 75.1°, which corresponded to (110), (002), (111), (202), (020), (202), (113), (311), (113), (311), and (222) planes, respectively (Fig. 1A).[22] Fig. 1B shows the diffractograms of bare CNTs and Cu loaded onto CNT (Cu/CNT) catalysts with different weight loadings (1–5 wt%). Two main peaks were observed at 2θ = 25.3° (002) and 43° (100) for the bare CNTs (Fig. 1B(a)), indicating that the structural ordering of CNTs is similar to the results reported in the literature.[23–26] The intensity of both peaks decreased with increasing Cu loading (Fig. 1B(b–d)), which demonstrated that the incorporation of Cu affected the structural arrangement of the CNT.[27] The peaks for CuO were clearly observed in the 5 wt% Cu/CNT (Fig. 1B(c and d)), suggesting its good distribution on the surface of CNTs.[28,29]

The morphological structure of the catalysts was then examined by TEM and the results are displayed in Fig. 2. A relatively uniform structure with a rather smooth and well-graphitized parallel wall of pristine MWCNTs was observed (Fig. 2A–C), with an estimated outer diameter of 20–30 nm.[30] Fig. 2D–F shows the images of the 3 wt% Cu/CNT, in which the CNT seems to twist and bend to each other where CuO is deposited on the CNT.[31] The resulting surface defects on the amorphous carbon layers are expected to be advantageous for the photoactivity of the catalyst.

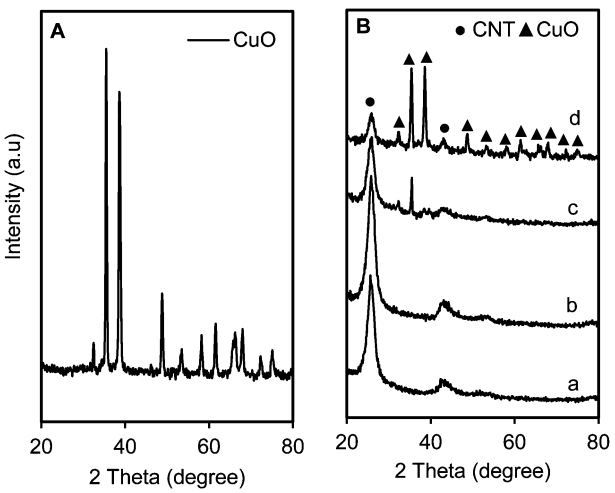

Fig. 1 XRD patterns of (A) CuO and (B) Cu/CNTs (a) CNT (b) 1 wt% Cu/CNTs (c) 3 wt% Cu/CNTs (d) 5 wt% Cu/CNTs.

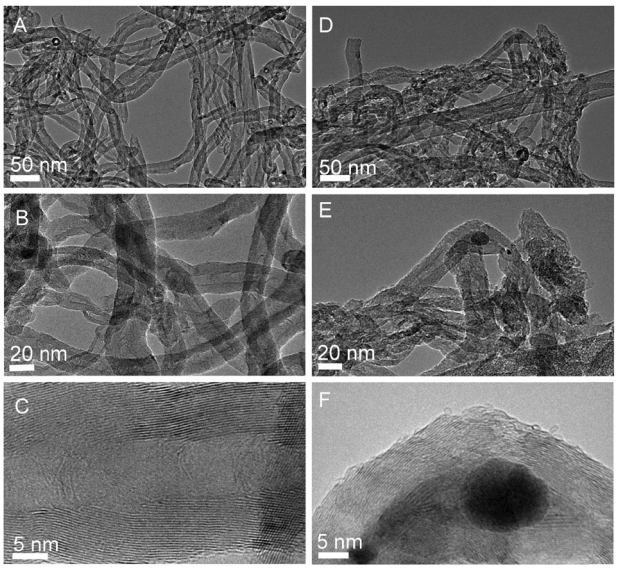

Fig. 2 TEM image of CNTs (A–C) and 3 wt% Cu/CNTs (D–F).

Table 1 The textural properties of the catalysts

Catalyst	Surface area ($m^2\ g^{-1}$)	Pore volume ($cm^3\ g^{-1}$)	Average pore size (nm)
CNT	180	1.05	52.3
1 wt% Cu/CNT	201	0.947	4.89
3 wt% Cu/CNT	205	0.764	4.57
5 wt% Cu/CNT	197	0.879	4.89
CuO	2.00	0.011	6.08

Next, the catalysts were subjected to N_2 adsorption–desorption in order to get more information on their specific surface area, pore volume and pore size distribution. The plot of the Cu/CNT demonstrated a type IV isotherm model with a H3 type hysteresis loop (Fig. S1A–D, ESI†), demonstrating the properties of materials with both micro- and macroporous structures.[32] The surface areas were 2, 180, 201, 205, and 197 $m^2\ g^{-1}$ for CuO, CNTs, 1 wt% Cu/CNTs, 3 wt% Cu/CNTs, and 5 wt% Cu/CNTs, respectively (Table 1).

It was observed that the surface area was increased with the introduction of Cu into the CNT. Most probably the larger pores of the CNT were blocked by the Cu nanoparticles to form numerous smaller pores as shown in Fig. S1E (ESI†).[33] The inset figure in Fig. S1E (ESI†) verified the presence of abundant smaller pores with increase in Cu loading onto the CNT. However, a further increase of Cu loading slightly reduced the surface area of the catalyst. This can be attributed to pore blocking by agglomerated copper species with the increased Cu loading.[34]

Chemical composition of the catalysts

Fig. 3 shows a magnification of the main bands of the FTIR spectra of CNTs and Cu/CNTs in the range of 1730 to 490 cm^{-1}. All catalysts exhibited bands attributed to a carbonyl group (1713 cm^{-1}), C=C vibration (1646 cm^{-1}), C–C vibration (1518 cm^{-1}), C–OH groups (1394 cm^{-1}), and C–O bonding (1022 cm^{-1}) vibration (Fig. 3A–E).[35–37] The results show that

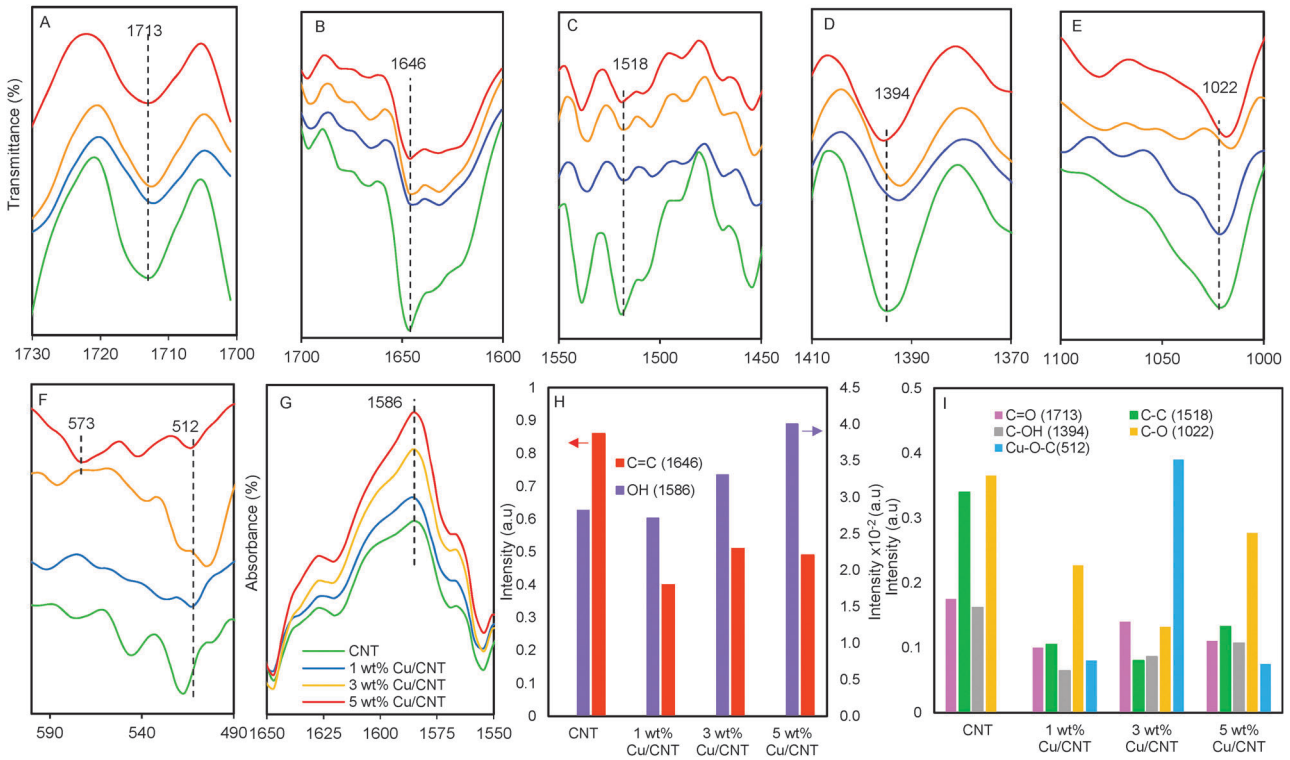

Fig. 3 (A–G) FTIR spectra of CNTs, and 1–5 wt% Cu/CNTs, (H and I) summary of all peaks intensities based on pristine CNTs.

the carbonaceous structure was retained despite the introduction of Cu, implying that no major changes occurred in the CNT. For a better view, the intensity of those bands is summarized in Fig. 3H and I. It could be observed that almost all bands decreased to some degree after the addition of Cu, signifying that possible interactions occurred between those functional groups with the Cu species, while a new band appeared at 512 cm^{-1} (Fig. 3F) when Cu was introduced onto the CNT which seemingly corresponded to the Cu–O–C vibration.[38] In order to study the possible interaction between Cu and hydroxyl groups on the CNT, the catalyst was also evacuated at 623 K for 1 h prior to IR measurements to remove the physisorbed water and the spectra are shown in Fig. 3G. The 5 wt% Cu/CNT showed the highest increase at band 1586 cm^{-1}, indicating the greatest number of –OH groups compared to other Cu/CNTs. This is most probably due to the hydroxylation of C=C groups, which easily occurred under these conditions in the presence of perchlorate ions from tetra ethyl ammonium perchlorate (TEAP) during electrolysis. Similar cases have been reported in the hydroxylation of alkenes under mild conditions using alkaline permanganate and osmium tetroxide.[39] In addition, the decrease at band 1022 cm^{-1} showed the possible ring opening of epoxy groups that already exist in the pristine CNT to form more –OH groups under the same conditions.[40] An oxidative cleavage of C–C bonds also occurred to form carbonyl groups with increasing Cu content, as reported in the literature when diols were treated with sodium periodate to form new carbon–oxygen double bonds.[41] This was confirmed by the decrease of the band at 1518 cm^{-1} and the increase of the band at 1713 cm^{-1} especially for 3 wt% Cu/CNTs. A significant increase at band 512 cm^{-1} and shift to 503 cm^{-1} were also demonstrated by the 3 wt% Cu/CNT, signifying that a stronger interaction of Cu^{2+} ions with the oxygen atoms occurred for this catalyst during electrolysis to form the Cu–O–C bonds.[42,43]

However, the excess of electrolyzed Cu^{2+} ions in the preparation of 5 wt% Cu/CNTs seemed to favor the formation of CuO nanoparticles instead of Cu–O–C bonds, as confirmed by the appearance of a new band at 573 cm^{-1} which corresponded to the vibration of Cu(II)O oxide.[44] Similar phenomena were observed in our previous work when electrolyzed metal ions were introduced into zeolite and silica.[17–19]

Next, the interaction between CuO and the CNT was further investigated by XPS using the 3 wt% Cu/CNT and compared with the pristine CNT (Fig. 4). The peak for the C 1s signal at 284.5 eV (Fig. 4A) showed a decrease when CuO was incorporated onto the CNT (Fig. 4B). It was observed from a Gaussian curve-fitting that the sp^2, sp^3, C–O, and O–C=O bonds were decreased, while the C=O bonds increased and a new peak for C–Cu appeared, supporting the FTIR data which verified the interaction between the CNT and Cu species. In the case of the O 1s signal shown in Fig. 4C, an increase in the intensity of the overall peak was perceived (Fig. 4D), mainly due to the presence of components aroused from the interaction between copper and oxygen as well as the increase in carbonyl groups. In parallel with the FTIR results, the peaks for C–O, O–C=O, and –OH decreased to form a new Cu–O peak.

Next, the catalysts were subjected to ESR in order to study their electronic structure with unpaired electrons (Fig. 5A).

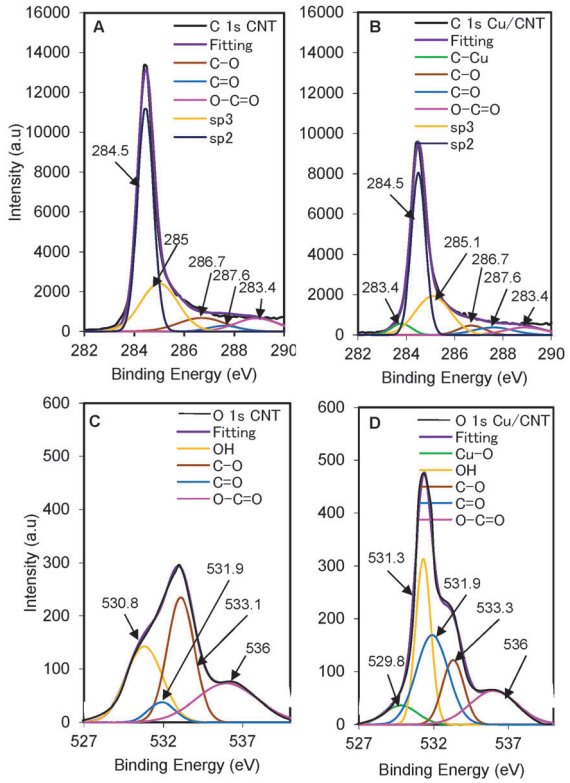

Fig. 4 XPS spectra of (A) C 1s CNTs, (B) C 1s Cu/CNTs, (C) O 1s CNTs, and (D) O 1s for Cu/CNTs.

In fact, the *g*-value obtained from the ESR has been used to clarify the properties of metal–carbon nanotubes and their defect states.[45] It was found that the *g*-value for the pristine CNT was 2.01, which is in agreement with the *g*-value of 2.01–2.02 reported by most other researchers.[46,47] This is attributed to the interaction between the conducting electrons in the CNT trapped at defects and magnetic ion sites.[48] The strong ESR signal observed with symmetric resonance suggests that the abundant unpaired electrons on the surface of the pristine CNT as well as the defect sites originated from opened tips or defects in the nanotube lattice, which primarily consists of sp^3 defects as well as C=O and C–OH groups.[41] It was observed that the addition of Cu onto the CNT considerably reduced the ESR signal intensity, suggesting that the interactions between Cu and the CNT occurred preferentially at the defect sites along the CNT backbone, rather than at the tip.[41] The shift in the *g*-value to 2.11 for the 3 wt% CuO/CNT can be interpreted as a shift in electron density along the CNT backbone due to the interaction with the Cu species decorated along the surface of the CNT, which is similar to that reported for the attachment of Pt nanoparticles to the SWCNT.[41] A large metal content is known to cause rapid relaxation of the conducting electrons rendering some of the nanotubes unobservable.[49] Herein, it could be deduced that the functional groups serve as preferred nucleation points for capturing Cu^{2+} ions from electrolyzed solution, yielding CNTs that are uniformly decorated with Cu.

Based on the characterization data above, the structure of the Cu/CNT catalyst was proposed as illustrated in Fig. 5B. The FTIR, XPS and ESR analysis confirmed the presence of hydroxyl and carboxyl groups on the pristine CNT. Introduction of Cu^{2+} ions from the anode during electrolysis led the oxygen atoms from both functional groups to interact with Cu, which was verified by the intensity changes of those related peaks in the FTIR and XPS spectra. The significant reduction of the ESR spectrum of the CNT by the addition of Cu up to 3 wt% and above supported the fact that the unpaired electrons of oxygen atoms from both –OH and –COOH groups are supposed to be occupied by the Cu species. The decrease in the surface area and pore volume also verified the deposition of Cu species onto the surface of CNTs.

Photocatalytic activity in the degradation of *p*-chloroaniline

The photoactivity of the catalysts was examined in the degradation of PCA and the results are shown in Fig. 6A. All of the catalysts were tested both in the dark (the first 60 min) and under UV light at pH 7 (Fig. S2, ESI†). It could be observed that photolysis

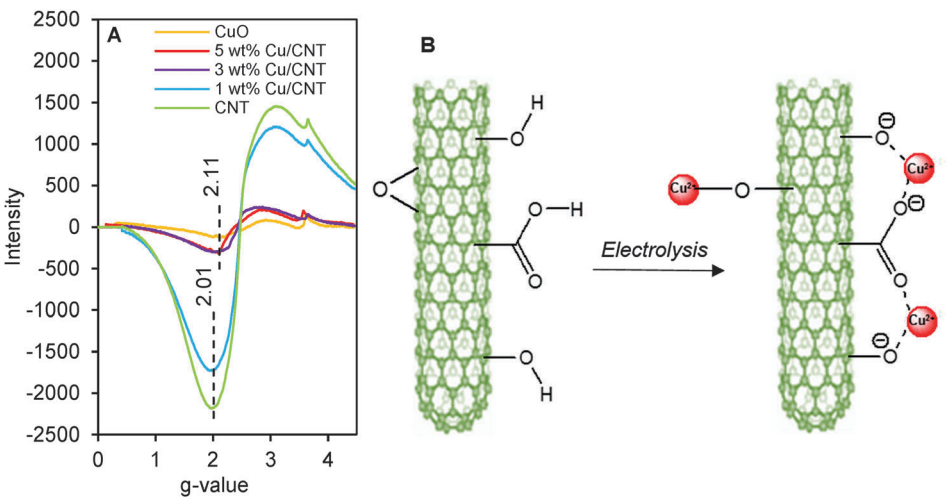

Fig. 5 (A) ESR spectra of all catalysts, (B) proposed structure of Cu/CNT.

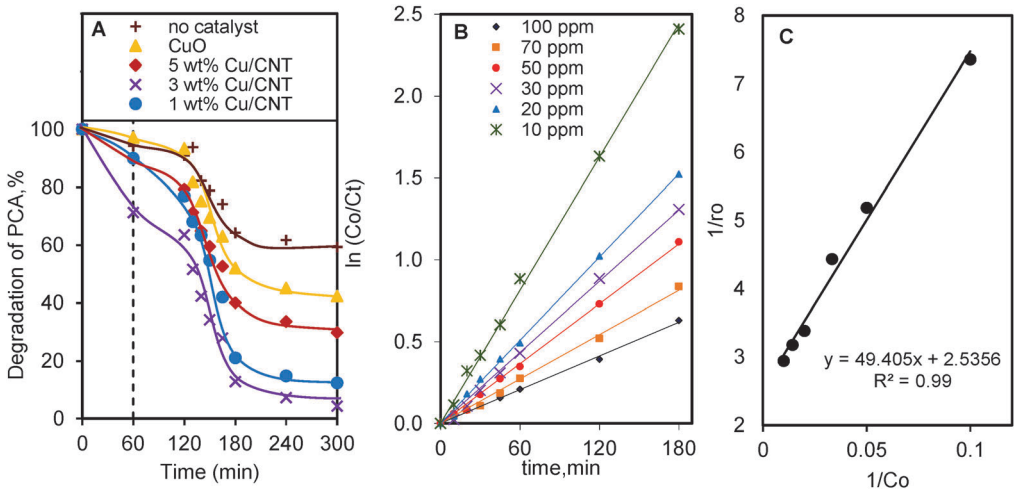

Fig. 6 (A) Performance of the catalysts in the photodegradation of PCA, (B) kinetic studies of photodegradation and (C) relationship between 1/ro and 1/Co at different concentrations of PCA.

resulted in only 40% degradation after 6 h of reaction, while the addition of 0.375 g L^{-1} CuO (Fig. S3, ESI†) was able to improve the degradation up to 60%. However, a significant enhancement was seen when 1 wt% and 3 wt% CuO were added into the CNT with 82 and 96% degradation achieved, respectively, whereas a further increase of Cu loading to 5 wt% decreased the degradation efficiency to 76%. The greater interaction between Cu and the CNT in the form of Cu–O–C bonds possessed by the 3 wt% CuO/CNT most probably played an important role in achieving the highest level of photodegradation.[18,27,43,50] Indeed, the higher surface area as well as smaller pore volume and pore size of the 3 wt% CuO/CNT also contributed to its higher activity. The Cu species that were on the surface of CNTs were easily exposed to UV light and generated more active sites. In contrast, the excess dispersion of less active CuO on the surface of the 5 wt% CuO/CNT might have impeded the photodegradation.[18]

Kinetics study

In order to determine the photodegradation rate, a series with initial concentrations of PCA ranging from 10 to 100 mg L^{-1} was performed over 0.375 g L^{-1} of 3 wt% CuO/CNTs at pH 7. A Langmuir–Hinshelwood (L–H) model was fitted to accommodate reactions occurring at a solid–liquid interface and the result is shown in Fig. 6B. The plot of $\ln(C_0/C_t)$ *vs.* irradiation time verified that the reaction process approximately followed the pseudo-first order kinetic model,[51] which is expressed by the simplified equation below,

$$\ln\frac{C_0}{C_t} = kt \qquad (3)$$

where k is the pseudo-first order rate constant and C_0 and C_t are the concentrations of PCA at initial time and time t, respectively.

A significant effect of CuO/CNTs on the photodegradation of PCA was revealed by the k values listed in Table 2. It is observed that the k value increased inversely with initial concentration, demonstrating that the saturation of PCA on the catalyst surface lowered the photodegradation efficiency. Similar results were reported by Shivaraju *et al.* when studying the effect of organic substrate concentration on the photo-degradation of sewage water by a TiO_2-based heterogeneous photocatalyst.[52] Additionally, the L–H kinetic model was plotted and the results are shown in Fig. 6C. The line with an intercept of $1/k_r$ and $1/k_{LH}$ was obtained from the L–H kinetic equation as follows,

$$\frac{1}{r_0} = \left(\frac{1}{k_r k_{LH}}\right)\left(\frac{1}{C_0}\right) + \frac{1}{k_r} \qquad (4)$$

where r_0 is the initial reaction rate, k_r is the reaction rate constant (mg L^{-1} min^{-1}), k_{LH} is the adsorption coefficient of the reactant (L mg^{-1}) and C_0 is the initial concentration of PCA (mg L^{-1}). The calculated values of k_r and k_{LH} were 0.3944 mg L^{-1} min^{-1} and 0.0513 L mg^{-1}, respectively, indicating that PCA adsorption was the controlling step of the process. This is similar to the kinetics study obtained by the photo-degradation of chlorophenol using colloidal a-FeOOH supported by mesostructured silica nanoparticles.[53]

Table 2 Kinetic parameters for PCA degradation on Cu/CNT catalysts

Initial concentration, C_0 (mg L^{-1})	$k \times 10^{-3}$ (min^{-1})	R^2	$r_0 \times 10^{-1}$ (mg L^{-1} min^{-1})
10	13.6	0.998	1.36
20	8.50	0.999	1.70
30	7.20	0.997	2.16
50	6.10	0.998	3.05
70	4.50	0.996	3.15
100	3.40	0.998	3.40

Proposed mechanism of the photocatalytic activity of Cu/CNTs in the degradation of PCA

In order to investigate the mechanism of photocatalytic activity of the Cu/CNT in the degradation of PCA, the effect of scavenging agents was examined: sodium oxalate, sodium bicarbonate, and potassium peroxydisulphate, with roles as scavengers for holes, OH radicals at the catalyst surface, and electrons, respectively.[54–56] As shown in Fig. 7A, the extent of degradation over the 3 wt%

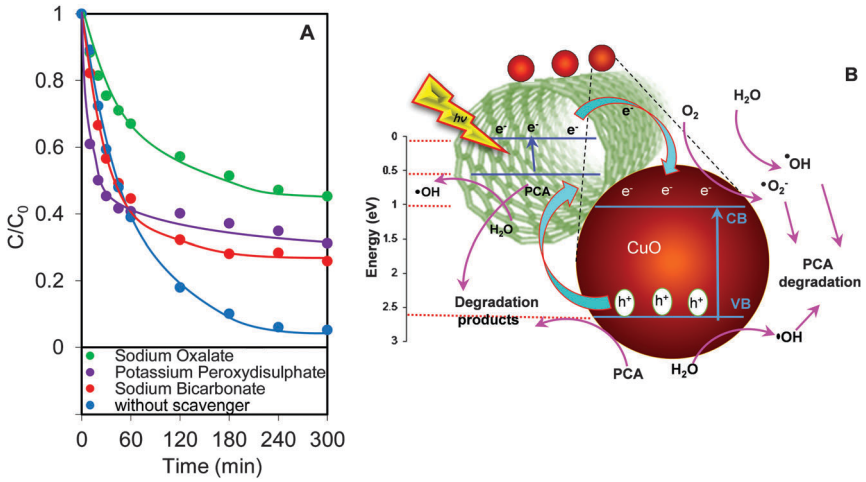

Fig. 7 (A) Effect of scavengers on the degradation of PCA and (B) the proposed reaction mechanism over the Cu/CNT photocatalyst.

Cu/CNT was 55%, 69%, 74%, and 96% for scavengers of holes, electrons, OH radicals, and without scavengers, respectively. Thus, it could be deduced that the holes played an important role in degradation over Cu/CNTs.

It has been reported that the band gap of SWCNTs is 0.5 eV, and the highest occupied molecular orbital (HOMO) and lowest unoccupied molecular orbital (LUMO) potentials of SWCNTs are 0.2 and 0.7 eV, respectively.[57] Based on previous studies, the conduction band (CB) and valence band (VB) edge potentials of CuO were at 1.0 and 2.7 eV, respectively.[58] Considering the results from the effect of scavengers above, the VB electrons in both the CNT and CuO were excited to produce photogenerated electron–hole pairs when the Cu/CNT catalysts were exposed to UV light (Fig. 7B).[59,60] The electrons generated were able to transfer from the CNT to the CuO phase, while the photoinduced holes on the surface of CuO could transfer easily to the CNT through the heterojunctions, since the VB edge potential of CuO (2.7 eV) is more positive than the LUMO of the CNT (0.7 eV). This phenomenon could efficiently reduce the recombination rate of the electron–hole pairs, and thus significantly improve the photoactivity of the Cu/CNT compared to pure CuO. The separated electrons and holes could form reactive oxygen species with O_2 and H_2O, leading to the formation of $O_2^{\bullet -}$ and $OH^{\bullet}$, respectively, which are responsible for the degradation of PCA.

The degradation of PCA was further investigated by GC-MSD and the mechanism is proposed in Fig. 8. It can be seen from Fig. S4 (ESI†) that the chromatographic structure of the species with *m*/*z* 127 decreased over time, signifying the possible PCA degradation into other compounds. Firstly, PCA might be transformed into its intermediates *via* two possible ways; dechlorination to form aniline or reaction with CO_2 from the atmosphere to form 4-chloroformanilide. Subsequently, combination of both compounds gave 1-(4-chlorophenyl)-3-phenylurea,[2] which then further degraded to 2-(2-aminopropanoylamino)-4-methylpentanoic acid. After several hours, 4-methylpentanoic acid and methylbutylamine were detected before being finally mineralized into CO_2 and H_2O (Fig. S5, ESI†).

Conclusions

In this study, Cu/CNT catalysts were prepared *via* an electrochemical method and their physicochemical properties were

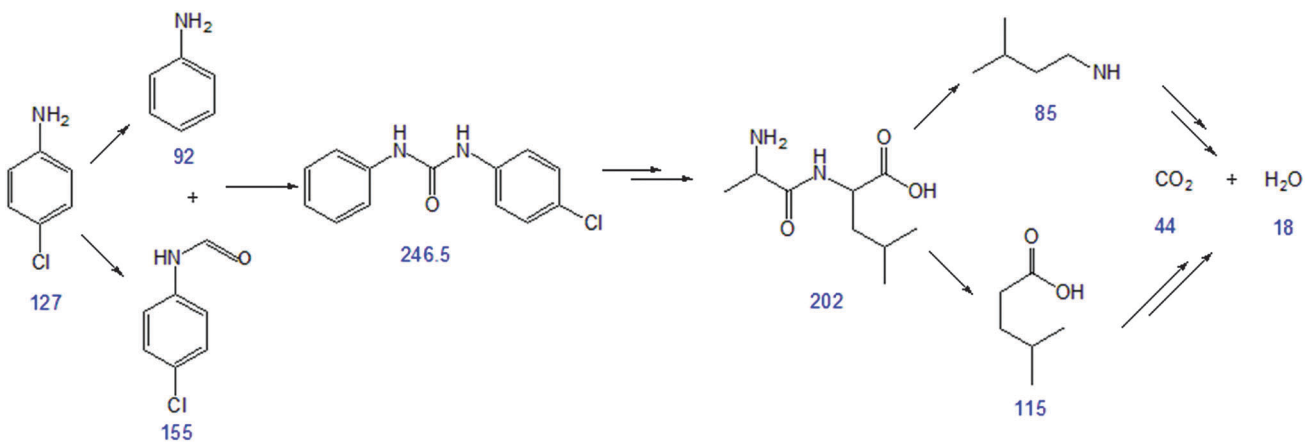

Fig. 8 Proposed mechanism for the photodegradation pathway of PCA.

studied by XRD, TEM, N_2 adsorption–desorption, FTIR, XPS, and ESR. The XRD results showed that the Cu was well distributed on the CNT, which reduced the surface area of the catalyst. The decrease in the number of C=C, C–C, hydroxyl, and carboxyl groups with increasing amounts of Cu demonstrated by FTIR suggests the possible interactions between them and Cu^{2+} ions to form Cu–O–C bonds during electrolysis. This was further confirmed by the XPS data, which showed a decrease in sp^2, sp^3, C–O and O–C=O peaks. The significant reduction in the ESR spectra of catalysts by the addition of Cu up to 3 wt% and above supported the fact that the unpaired electrons of oxygen atoms from both –OH and –COOH groups were employed by the Cu, indicating that the interaction between Cu and the CNT occurred at the sp^3 defect sites, and C=O and C–OH along the CNT backbone. The highest numbers of Cu–O–C bonds possessed by 0.375 g L^{-1} of 3 wt% Cu/CNT demonstrated the best degradation performance of 10 mg L^{-1} of PCA (96%) under UV light irradiation within 5 h of reaction at 27 °C and neutral pH. The kinetic studies showed that the degradation followed the pseudo-first order model and the surface reaction was the controlling step. Based on the effect of scavenger studies, the VB electrons in both the CNT and CuO were excited to produce photogenerated electron–hole pairs when the Cu/CNT catalysts were exposed to UV light. The electrons generated are able to transfer from the CNT to the CuO phase, while the photoinduced holes on the surface of CuO could transfer easily to the CNT through the heterojunctions, since the VB edge potential of CuO is more positive than the LUMO of the CNT. This phenomenon could efficiently reduce the recombination rate of the electron–hole pairs, and thus significantly improve the photoactivity of the Cu/CNT catalysts compared to pure CuO.

Acknowledgements

The authors are grateful for the financial support from the Research University Grant from Universiti Teknologi Malaysia (Grant No. 07H06) and the awards of the MyPhD Scholarship (Nur Farahain Khusnun) from the Ministry of Higher Education Malaysia.

References

1 F. Gosetti, M. Bottaro, B. Gianotti, M. Mazzucco, P. Frascarolo, D. Zampieri, C. Oliveri, A. Viarengo and M. C. Gennaro, *Environ. Pollut.*, 2010, **158**, 592–598.
2 I. Hussain, Y. Zhang, S. Huang and X. Du, *Chem. Eng. J.*, 2012, **203**, 269–276.
3 T. Ana, L. Suna, G. Li, Y. Gao and G. Ying, *Appl. Catal., B*, 2011, **102**, 140–146.
4 C. Antonetti, M. Oubenali, A. M. R. Galletti, P. Serp and G. Vannucci, *Appl. Catal., A*, 2012, **421–422**, 99–107.
5 P. Hongsawat and A. S. Vangnai, *J. Hazard. Mater.*, 2011, **186**, 1300–1307.
6 M. Sanchez, H. Wolfger and N. Getoff, *Radiat. Phys. Chem.*, 2002, **65**, 611–620.
7 L. P. Bakhaeva, G. K. Vasilyeva, E. G. Surovtseva and V. M. Mukhin, *Microbiology*, 2003, **70**, 277–284.
8 R. Jusoh, A. A. Jalil, S. Triwahyono and N. H. N. Kamarudin, *RSC Adv.*, 2015, **5**(13), 9727–9736.
9 N. R. Srinivasan, P. Majumdar, N. K. R. Eswar and R. Bandyopadhyaya, *Appl. Catal., A*, 2015, **498**, 107–116.
10 R. M. Mohamed and M. M. Mohamed, *Appl. Catal., A*, 2008, **340**, 16–24.
11 N.-E. Alireza and Z. Salimi, *Appl. Catal., A*, 2010, **390**, 110–118.
12 N.-E. Alireza and K.-S. Maryam, *Appl. Catal., A*, 2014, **477**, 83–89.
13 K. Dong, X. Ma, H. Zhang and G. Lin, *J. Nat. Gas Chem.*, 2006, **15**(1), 28–37.
14 N. F. Jaafar, A. A. Jalil, S. Triwahyono, M. Nazlan, M. Muhid, N. Sapawe, M. A. H. Satar and H. A. Nazlan, *Chem. Eng. J.*, 2012, **191**, 112–122.
15 A. A. Jalil, M. A. H. Satar, S. Triwahyono, H. D. Setiabudi, N. H. N. Kamarudin, N. F. Jaafar, N. Sapawe and R. Ahamad, *J. Electroanal. Chem.*, 2013, **701**, 50–58.
16 N. W. C. Jusoh, A. A. Jalil, S. Triwahyono and C. R. Mamat, *Appl. Catal., A*, 2015, **492**, 169–176.
17 G. Cheng, I. Calizo and A. R. H. Walker, *Carbon*, 2015, **81**, 678–687.
18 A. A. Jalil, N. Kurono and M. Tokuda, *Synthesis*, 2002, 2681–2686.
19 A. A. Jalil, N. Kurono and M. Tokuda, *Tetrahedron*, 2002, **58**, 7477–7484.
20 A. A. Jalil, N. Kurono and M. Tokuda, *Synlett*, 2001, 1944–1946.
21 Y.-P. Chang, C.-L. Ren, J.-C. Qu and X.-G. Chen, *Appl. Surf. Sci.*, 2012, **261**, 504–509.
22 D. Manoj, D. R. Kumar and J. Santhanalakshmi, *Appl. Nanosci.*, 2012, **2**, 223–230.
23 D.-N. Bui, S.-Z. Kang, Q. Lixia, X.-Q. Li and M. Jin, *Appl. Surf. Sci.*, 2013, **266**, 288–293.
24 J. Tingshun, L. Zhang, M. Ji, Q. Wang, Q. Zhao, X. Fu and H. Yin, *Particuology*, 2013, **11**, 737–742.
25 L. Jiangab and L. Gao, *J. Mater. Chem.*, 2005, **15**, 260–266.
26 H. Xu, C. Wang, Y. Song, J. Zhu, Y. Xu, J. Yan, Y. Song and H. Li, *Chem. Eng. J.*, 2014, **241**, 35–42.
27 N. W. C. Jusoh, A. A. Jalil, S. Triwahyono, H. D. Setiabudi, N. Sapawe, M. A. H. Satar, A. H. Karim, N. H. N. Kamarudin, R. Jusoh, N. F. Jaafar, N. Salamun and J. Efendi, *Appl. Catal., A*, 2013, **468**, 276–287.
28 W.-C. Fang, *Nanoscale Res. Lett.*, 2010, **5**, 68–73.
29 D. Zhang, H. Mai, L. Huang and L. Shi, *Appl. Surf. Sci.*, 2010, **256**, 6795–6800.
30 A. H. Karim, A. A. Jalil, S. Triwahyono, N. H. N. Kamarudin and A. Ripin, *J. Colloid Interface Sci.*, 2014, **421**, 93–102.
31 Y.-J. Xu, Y. Zhuang and X. Fu, *J. Phys. Chem. C*, 2010, **114**, 2669–2676.
32 J. Wei, J. Jia, F. Wu, S. Wei, H. Zhou, H. Zhang, J.-W. Shin and C. Liu, *Biomaterials*, 2010, **31**, 1260–1269.
33 A. Tavasoli, S. Karimi, H. Nikookar and H. Fadakar, *Iran. J. Chem. Chem. Eng.*, 2013, **32**, 11–19.

34 A. Rachel, V. D. Kumari, R. Subramanian, K. V. R. Chary and P. K. Rao, *Indian J. Chem.*, 2004, **43A**, 1172–1180.

35 S. Zeng, L. Zhang, N. Jiang, M. Gao, X. Zhao, Y. Yin and H. Su, *J. Power Sources*, 2015, **293**, 1016–1023.

36 S.-Z. Kang, D.-E. Yin, X. Li and J. Mu, *Colloids Surf., A*, 2011, **384**, 363–367.

37 X.-L. Ling, Y.-Z. Wei, L.-M. Zou and S. Xu, *Colloids Surf., A*, 2012, **421**, 9–15.

38 B. Zhao, P. Liu, H. Zhuang, Z. Jiao, T. Fang, W. Xu, B. Lu and Y. Jiang, *J. Mater. Chem. A*, 2013, **1**, 367–373.

39 J. G. Smith, *Organic Chemistry*, Mc Graw Hill, New York, 2nd edn, 2008.

40 Q. Cheng, R. Liang, B. Wang and C. Zhang, *U.S. Pat.*, 2013/0264521 A1, 2013.

41 L. Dennany, P. Sherrell, J. Chen, P. C. Innis, G. G. Wallace and A. I. Minett, *Phys. Chem. Chem. Phys.*, 2010, **12**, 4135–4141.

42 N. F. M. Salleh, A. A. Jalil, S. Triwahyono, J. Efendi, R. R. Mukti and B. H. Hameed, *Appl. Surf. Sci.*, 2015, **349**, 485–495.

43 S. M. Sidik, A. A. Jalil, S. Triwahyono, T. A. T. Abdullah and A. Ripin, *RSC Adv.*, 2015, **5**, 37405–37414.

44 S. B. Khan, M. Faisal, M. M. Rahman, I. A. Abdel-Latif, A. A. Ismail, K. Akhtar, A. Al-Hajry, A. M. Asiria and K. A. Alamry, *New J. Chem.*, 2013, **37**, 1098–1104.

45 M. Chipara, J. M. Zaleski, D. Hui, C. Du and N. Pan, *J. Polym. Sci., Part B: Polym. Phys.*, 2005, **43**, 3406–3412.

46 O. Chauvet, L. Forro, W. Bacsa, D. Ugarte, B. Doudin and W. A. de Heer, *Phys. Rev. B: Condens. Matter Mater. Phys.*, 1995, **52**, R6963.

47 F. Beuneu, C. l'Huillier, J.-P. Salvetat, J.-M. Bonard and L. Forró, *Phys. Rev. B: Condens. Matter Mater. Phys.*, 1999, **59**, 5945.

48 M. Deborah, A. Jawahar, T. Mathavan, M. K. Dhas and A. M. F. Benial, *Fullerenes, Nanotubes, Carbon Nanostruct.*, 2014, **23**, 649–657.

49 K. Shen, D. L. Tierney and T. Pietra, *Phys. Rev. B: Condens. Matter Mater. Phys.*, 2003, **68**, 165418.

50 N. W. C. Jusoh, A. A. Jalil, S. Triwahyono, A. H. Karim, N. F. M. Salleh, N. H. R. Annuar, N. F. Jaafar, M. L. Firmansyah, R. R. Mukti and W. W. Ali, *Appl. Surf. Sci.*, 2015, **330**, 10–19.

51 N. F. Jaafar, A. A. Jalil, S. Triwahyono, J. Efendi, R. R. Mukti, R. Jusoh, N. W. C. Jusoh, A. H. Karim, N. F. M. Salleh and V. Suendo, *Appl. Surf. Sci.*, 2015, **338**, 75–84.

52 H. P. Shivaraju, *Int. J. Environ. Sci.*, 2011, **1**(5), 911–923.

53 R. Jusoh, A. A. Jalil, S. Triwahyono, A. Idris and M. Y. Noordin, *Sep. Purif. Technol.*, 2015, **149**, 55–64.

54 R. Jusoh, A. A. Jalil, S. Triwahyono, A. Idris, S. Haron, N. Sapawe, N. F. Jaafar and N. W. C. Jusoh, *Appl. Catal., A*, 2014, **469**, 33–44.

55 M. Mehrvar, W. A. Anderson and M. M. Young, *Int. J. Photoenergy*, 2001, **3**, 187–191.

56 A. Syoufian and K. Nakashima, *J. Colloid Interface Sci.*, 2008, **317**, 507–512.

57 Z. K. Horastani, S. J. Hashemifar, S. M. Sayedi and M. H. Sheikhi, *Int. J. Hydrogen Energy*, 2013, **38**, 13680–13686.

58 Y. Xu and M. A. A. Schoonen, *Am. Mineral.*, 2000, **85**, 543–556.

59 L. Zhang, D. Jing, X. She, H. Liu, D. Yang, Y. Lu, J. Li, Z. Zheng and L. Guo, *J. Mater. Chem. A*, 2014, **2**, 2071–2078.

60 Z. Xiu, H. Bo, Y. Wu and X. Hao, *Appl. Surf. Sci.*, 2014, **289**, 394–399.